Dataset Distillation in Large Data Era

Anonymous authors
Paper under double-blind review

Abstract

Dataset distillation or condensation aims to generate a smaller but representative subset from a large dataset, which allows a model to be trained more efficiently, meanwhile evaluating on the original testing data distribution to achieve decent performance. Previous decoupled methods like SRe^{2}L simply use a unified gradient update scheme for synthesizing data from Gaussian noise, while, we notice that the initial several update iterations will determine the final outline of synthesis, thus an improper gradient update strategy may dramatically affect the final generation quality. To address this, we introduce a simple yet effective *global-to-local* gradient refinement approach enabled by curriculum data augmentation (`CDA`) during data synthesis. The proposed framework achieves the current published highest accuracy on both large-scale ImageNet-1K and 21K with 63.2% under IPC (Images Per Class) 50 and 36.1% under IPC 20, using a regular input resolution of 224×224. The proposed model outperforms the current state-of-the-art methods like SRe^{2}L, TESLA, and MTT by more than 4% Top-1 accuracy on ImageNet-1K/21K and for the first time, reduces the gap to its full-data training counterparts to less than absolute 15%. Moreover, this work represents the inaugural success in dataset distillation on the larger-scale ImageNet-21K dataset under the standard 224×224 resolution. Our distilled ImageNet-21K dataset of 20 IPC, 2K recovery budget is available anonymously at link.

1 Introduction

Dataset distillation or condensation (Wang et al., 2018) has attracted considerable attention across various fields of computer vision (Cazenavette et al., 2022b; Cui et al., 2023; Yin et al., 2023) and natural language processing (Sucholutsky & Schonlau, 2021; Maekawa et al., 2023). This task aims to optimize the process of condensing a massive dataset into a smaller, yet representative subset, preserving the essential features and characteristics that would allow a model to learn from scratch as effectively from the distilled dataset as it would from the original large dataset. As the scale of data and models continue to grow, this *dataset distillation* concept becomes even more critical in the large data era, where datasets are often voluminous that they pose storage, computational, and processing challenges. Generally, dataset distillation can level the playing field, allowing researchers with limited computation and storage resources to participate in state-of-the-art foundational model training and application development, such as affordable ChatGPT (Brown et al., 2020; OpenAI, 2023) and Stable Diffusion (Rombach et al., 2022), in the current large data and large model regime. Moreover, by working with distilled datasets, there is potential to alleviate some data privacy concerns, as raw, personally identifiable data points might be excluded from the distilled version.

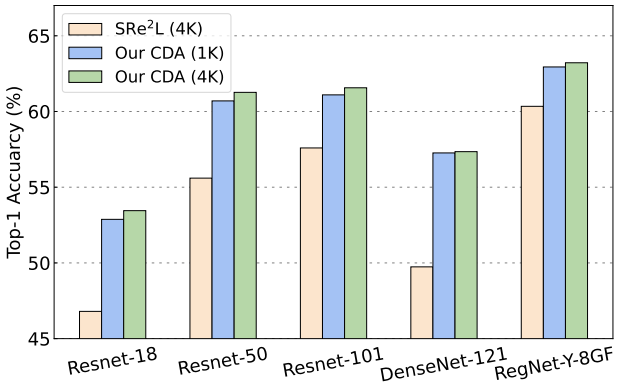

Figure 1: ImageNet-1K comparison with SRe^{2}L.

Recently, there has been a significant trend in adopting large models and large data across various research and application areas. Yet, many prior dataset distillation methods (Wang et al., 2018; Zhao et al., 2020;

Zhou et al., 2022; Cazenavette et al., 2022a; Kim et al., 2022a; Cui et al., 2023) predominantly target datasets like CIFAR, Tiny-ImageNet and downsampled ImageNet-1K, finding it challenging to scale their frameworks for larger datasets, such as full ImageNet-1K (Deng et al., 2009). This suggests that these approaches have not fully evolved in line with contemporary advancements and dominant methodologies.

In this study, we extend our focus even beyond the ImageNet-1K dataset, venturing into the uncharted territories of the full ImageNet-21K (Deng et al., 2009; Ridnik et al., 2021) at a conventional resolution of 224×224. This marks a pioneering effort in handling such a vast dataset for dataset distillation task. Our approach harnesses a straightforward yet effective global-to-local learning framework. We meticulously address each aspect and craft a robust strategy to effectively train on the complete ImageNet-21K, ensuring comprehensive knowledge is captured. Specifically, following a prior study (Yin et al., 2023), our approach initially trains a model to encapsulate knowledge from the original datasets within its dense parameters. However, we introduce a refined training recipe that surpasses the results of Ridnik et al. (2021) on ImageNet-21K. During the data recovery/synthesis phase, we employ a strategic learning scheme where partial image crops are sequentially updated based on the difficulty of regions: transitioning either from simple to difficult, or vice versa. This progression is modulated by adjusting the lower and upper bounds of the *RandomReiszedCrop* data augmentation throughout varying training iterations. Remarkably, we observe that this straightforward learning approach substantially improves the quality of synthesized data. In this paper, we delve into three learning paradigms for data synthesis linked to the curriculum learning framework. The first is the standard curriculum learning, followed by its alternative approach, reverse curriculum learning. Lastly, we also consider the basic and previously employed method of constant learning.

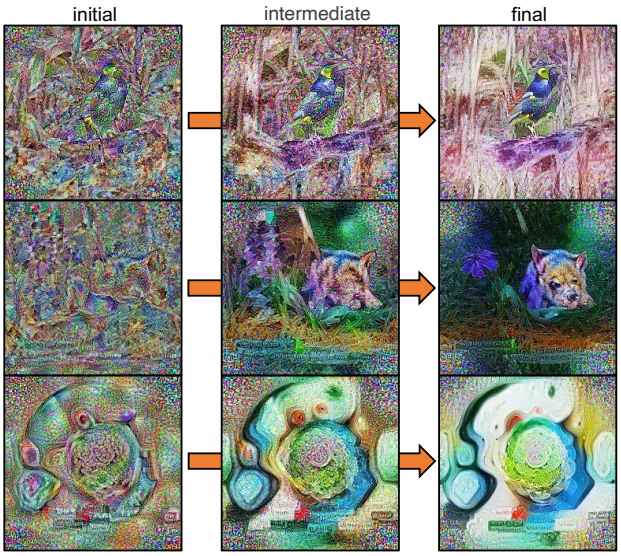

Figure 2: Motivation of our work. The left column is the synthesized images after a few gradient update iterations from Gaussian noise. Middle and right columns are intermediate and final synthesized images.

Motivation and Intuition. We aim to maximize the global informativeness of the synthetic data. Both SRe^{2}L (Yin et al., 2023) and our proposed approach utilize local mini-batch data's mean and variance statistics to match the global statistics of the entire original dataset, synthesizing data by applying gradient updates directly to the image. The impact of such a strategy is that the initial few iterations set the stage for the global structure of the ultimately generated image, as shown in Figure 2. Building upon the insights derived from the analysis, we can leverage the *global-to-local* gradient refinement scheme for more expressive synthesized data, in contrast, SRe^{2}L does not capitalize on this characteristic. Specifically, our proposed approach exploits this by initially employing large crops to capture a more accurate and complete outline of objects, for building a better foundation. As the process progresses, it incrementally reduces the crop size to enhance the finer, local details of the object, significantly elevating the quality of the synthesized data.

Global-to-local via Curriculum Sampling. *RandomResizedCrop* randomly crops the image to a certain area and then resizes it back to the pre-defined size, ensuring that the model is exposed to different regions and scales of the original image during training. As illustrated in Figure 3, the difficulty level of the cropped region can be controlled by specifying the lower and upper bounds for the area ratio of the crop. This can be used to ensure that certain portions of the image (small details or larger context) are present in the cropped region. If we aim to make the learning process more challenging, reduce the minimum crop ratio. This way, the model will often see only small portions of the image and will have to learn from those limited contexts. If we want the model to see a larger context more frequently, increase the minimum crop ratio. In this paper, we perform a comprehensive study on how the gradual difficulty changes by sampling strategy influence the optimization of data generation and the quality of synthetic data for dataset distillation. Our proposed curriculum data augmentation (`CDA`) is a heuristic and intuitive approach to simulate a *global-to-*

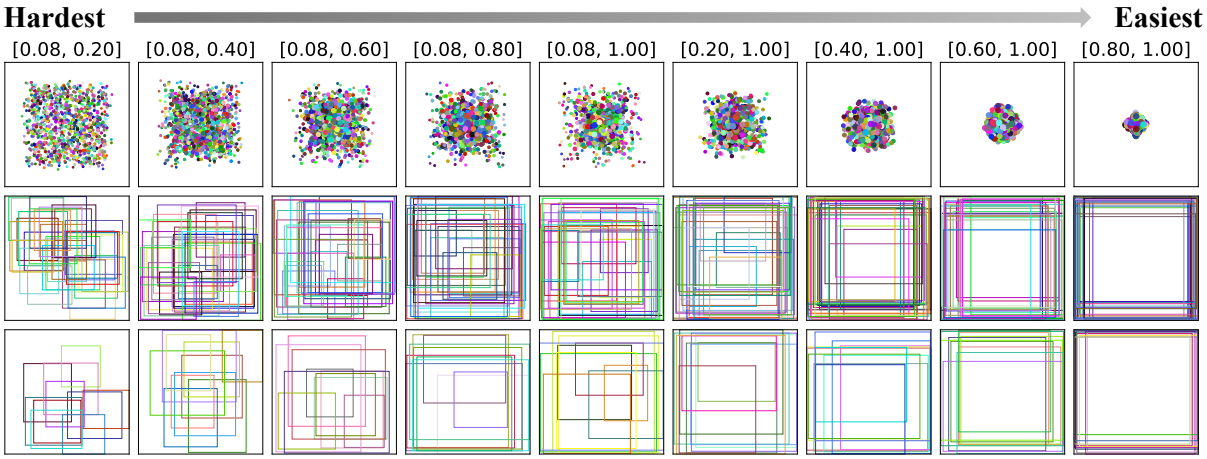

Figure 3: Illustration of crop distribution from different lower and upper bounds in *RandomResizedCrop*. The first row is the central points of bounding boxes from different sampling scale hyperparameters. The second and last rows correspond to 30 and 10 boxes of the crop distributions. In each row, from left to right, the difficulty of crop distribution is decreasing.

local learning procedure. Moreover, it is highly effective on large-scale datasets like ImageNet-1K and 21K, achieving state-of-the-art performance on dataset distillation.

The Significance of Large-scale Dataset Condensation. Large models trained on large-scale datasets tend to outperform smaller models and those trained on limited data (Dosovitskiy et al., 2020; Dehghani et al., 2023; OpenAI, 2023). They exhibit remarkable abilities in capturing intricate patterns and understanding nuanced contextual information, making them highly effective across diverse tasks and domains. These models are pivotal in solving complex industrial problems and enhancing the development of AI-driven products and services, thus driving economic growth and advancement. Consequently, it is essential to adapt dataset condensation or distillation approaches for these large-scale data scenarios to realize their true potential in both academic and industrial spheres.

We conduct extensive experiments on the CIFAR, Tiny-ImageNet, ImageNet-1K, and ImageNet-21K datasets. Employing a resolution of 224×224 and IPC 50 on ImageNet-1K, the proposed approach attains an impressive accuracy of 63.2%, surpassing all prior state-of-the-art methods by substantial margins. As illustrated in Figure 1, our proposed `CDA` outperforms SRe^{2}L by 4∼6% across different architectures under 50 IPC, on both 1K and 4K recovery budgets. When tested on ImageNet-21K with IPC 20, our method achieves a top-1 accuracy of 35.3%, which is closely competitive, exhibiting only a minimal gap compared to the model pre-trained with full data, at 44.5%, while using 50× fewer training samples.

Our contributions of this work:

- We propose a new curriculum data augmentation (CDA) framework enabled by *global-to-local* gradient update in data synthesis for large-scale dataset distillation.
- We are the first to distill the ImageNet-21K dataset, which reduces the gap to its full-data training counterparts to less than an absolute 15% accuracy.
- We conduct extensive experiments on CIFAR-100, Tiny-ImageNet, ImageNet-1K and ImageNet-21K datasets to demonstrate the effectiveness of the proposed approach.

2 Related Work

Dataset condensation or distillation strives to form a compact, synthetic dataset, retaining crucial information from the original large-scale dataset. This approach facilitates easier handling, reduces training time, and aims for performance comparable to using the full dataset. Prior solutions typically fall under four categories: *Meta-Model Matching* optimizes for model transferability on distilled data, with an outer-loop for

synthetic data updates, and an inner-loop for network training, such as DD (Wang et al., 2020), KIP (Nguyen et al., 2021), RFAD (Loo et al., 2022), FRePo (Zhou et al., 2022), LinBa (Deng & Russakovsky, 2022), and MDC (He et al., 2024); *Gradient Matching* performs a one-step distance matching between models, such as DC (Zhao et al., 2020), DSA (Zhao & Bilen, 2021), DCC (Lee et al., 2022), IDC (Kim et al., 2022b), and MP (Zhou et al., 2024a); *Distribution Matching* directly matches the distribution of original and synthetic data with a single-level optimization, such as DM (Zhao & Bilen, 2023), CAFE (Wang et al., 2022), HaBa (Liu et al., 2022a), KFS (Lee et al., 2022), DataDAM (Sajedi et al., 2023), FreD Shin et al. (2024), and GUARD (Xue et al., 2024); *Trajectory Matching* matches the weight trajectories of models trained on original and synthetic data in multiple steps, methods include MTT (Cazenavette et al., 2022b), TESLA (Cui et al., 2023), APM (Chen et al., 2023), and DATM (Guo et al., 2024).

Moreover, there are some recent methods out of these categories that have further improved the existing dataset distillation. SeqMatch (Du et al., 2023) reorganizes the synthesized dataset during the distillation and evaluation phases to extract both low-level and high-level features from the real dataset, which can be integrated into existing dataset distillation methods. Deep Generative Prior (Cazenavette et al., 2023) utilizes the learned prior from the pre-trained deep generative models to synthesize the distilled images. RDED (Sun et al., 2024) proposes a non-optimization method to concatenate multiple cropped realistic patches from the original data to compose the distilled dataset. D3M (Abbasi et al., 2024) condenses an entire category of images into a single textual prompt of latent diffusion models. SC-DD (Zhou et al., 2024b) proposes a self-supervised paradigm by applying the self-supervised pre-trained backbones for dataset distillation. EDC (Shao et al., 2024b) explores a comprehensive design space that includes multiple specific, effective strategies like soft category-aware matching and learning rate schedule to establishe a benchmark for both small and large-scale dataset distillation. Ameliorate Bias (Cui et al., 2024) studies the impact of bias within the original dataset on the performance of dataset condensation. It introduces a simple yet effective approach based on a sample reweighting scheme that utilizes kernel density estimation.

SRe^{2}L (Yin et al., 2023) is the first and mainstream framework to distill large-scale datasets, such as ImageNet-1K, and achieve significant performance. Thus, we consider it as our closest baseline. More specifically, SRe^{2}L proposes a decoupling framework to avoid the bilevel optimization of model and synthesis during distillation, which consists of three stages of squeezing, recovering, and relabeling. In the first squeezing stage, a model is trained on the original dataset and serves as a frozen pre-train model in the following two stages. During the recovering stage, the distilled images are synthesized with the knowledge recovered from the pre-train model. At the last relabeling stage, the soft labels corresponding to synthetic images are generated and saved by leveraging the pre-train model. Recently, distilling on large-scale datasets has received significant attention in the community, and many works have been proposed, including (Sun et al., 2023; Liu et al., 2023; Chen et al., 2023; Shao et al., 2024a; Zhou et al., 2024a; Wu et al., 2024; Abbasi et al., 2024; Zhou et al., 2024b; Shao et al., 2024b; Xue et al., 2024; Qin et al., 2024; Gu et al., 2023; Ma et al., 2024; Shang et al., 2024).

3 Approach

3.1 Preliminary: Dataset Distillation

The goal of dataset distillation is to derive a concise synthetic dataset that maintains a significant proportion of the information contained in the original, much larger dataset. Suppose there is a large labeled dataset $\mathcal{D}_o = \left\{\left(\boldsymbol{x}_1, \boldsymbol{y}_1\right), \ldots, \left(\boldsymbol{x}_{|\mathcal{D}_o|}, \boldsymbol{y}_{|\mathcal{D}_o|}\right)\right\}$, our target is to formulate a compact distilled dataset, represented as $\mathcal{D}_\mathrm{d} = \left\{\left(\boldsymbol{x}'_1, \boldsymbol{y}'_1\right), \ldots, \left(\boldsymbol{x}'_{|\mathcal{D}_d|}, \boldsymbol{y}'_{|\mathcal{D}_d|}\right)\right\}$, where $\boldsymbol{y}'$ is the soft label corresponding to synthetic data $\boldsymbol{x}'$, and $|\mathcal{D}_d| \ll |\mathcal{D}_o|$, preserving the essential information from the original dataset $\mathcal{D}_o$. The learning objective based on this distilled synthetic dataset is:

$$\boldsymbol{\theta}_{\mathcal{D}_d} = \arg\min_{\boldsymbol{\theta}} \mathcal{L}_{\mathcal{D}_d}(\boldsymbol{\theta}) \tag{1}$$

$$\mathcal{L}_{\mathcal{D}_d}(\boldsymbol{\theta}) = \mathbb{E}_{(\boldsymbol{x}', \boldsymbol{y}') \in \mathcal{D}_d}\Big[\ell(\phi_{\boldsymbol{\theta}_{\mathcal{D}_d}}(\boldsymbol{x}'), \boldsymbol{y}')\Big] \tag{2}$$

where ℓ is the regular loss function such as the soft cross-entropy, and $\phi_{\boldsymbol{\theta}_{\mathcal{D}_d}}$ is model. The primary objective of the dataset distillation task is to generate synthetic data aimed at attaining a specific or minimal performance

disparity on the original validation data when the same models are trained on the synthetic data and the original dataset, respectively. Thus, we aim to optimize the synthetic data $\mathcal{D}_d$ by:

$$\underset{\mathcal{D}_d, |\mathcal{D}_d|}{\arg\min} \left(\sup \left\{ \left| \ell \left(\phi_{\boldsymbol{\theta}_{\mathcal{D}_o}}(\boldsymbol{x}_{val}), \boldsymbol{y}_{val} \right) - \ell \left(\phi_{\boldsymbol{\theta}_{\mathcal{D}_d}}(\boldsymbol{x}_{val}), \boldsymbol{y}_{val} \right) \right| \right\}_{(\boldsymbol{x}_{val}, \boldsymbol{y}_{val}) \sim \mathcal{D}_o} \right) \tag{3}$$

where $(\boldsymbol{x}_{val}, \boldsymbol{y}_{val})$ are sample and label pairs in the validation set of the real dataset $\mathcal{D}_o$. Then, we learn $<\text{data}, \text{label}> \in \mathcal{D}_d$ with the corresponding number of distilled data in each class.

3.2 Dataset Distillation on Large-scale Datasets

Currently, the prevailing majority of research studies within dataset distillation mainly employ datasets of a scale up to ImageNet-1K (Cazenavette et al., 2022b; Cui et al., 2023; Yin et al., 2023) as their benchmarking standards. In this work, we are the pioneer in showing how to construct a strong baseline on ImageNet-21K (the approach is equivalently applicable to ImageNet-1K) by incorporating insights presented in recent studies, complemented by conventional optimization techniques. Our proposed baseline is demonstrated to achieve state-of-the-art performance over prior counterparts. We believe this provides substantial significance towards understanding the true impact of proposed methodologies on dataset distillation task and towards assessing the true gap with full original data training. We further propose a curriculum training paradigm to achieve a more informative representation of synthetic data. Following prior work in dataset distillation (Yin et al., 2023), we focus on the decoupled training framework, *Squeeze-Recover-Relabel*, to save computation and memory consumption on large-scale ImageNet-21K, the procedures are listed below:

Squeeze: Building A Strong Pre-trained Model on ImagNet-21K. To obtain a squeezing model, we use a relatively large label smooth of 0.2 together with Cutout (DeVries & Taylor, 2017) and RandAugment (Cubuk et al., 2020), as shown in Appendix B.4. This recipe helps achieve $\sim$2% improvement over the default training (Ridnik et al., 2021) on ImageNet-21K, as provided in Table 18.

Recover: Curriculum Training for Better Representation of Synthetic Data. A well-crafted curriculum data augmentation is employed during the synthesis stage to realize the global-to-local learning scheme and enhance the representational capability of the synthetic data. This step is crucial, serving to enrich the generated images by embedding more knowledge accumulated from the original dataset, thereby making them more informative. Detailed procedures will be further described in the following Section 3.3.

Relabel: Post-training on Larger Models with Stronger Training Recipes. Prior studies, such as TESLA (Cui et al., 2023), have encountered difficulties, particularly, a decline in accuracy when utilizing models of larger scale. This suggests that the synthetic data used is potentially inadequate for training larger models. Conversely, the data we relabel show improvement with the use of larger models combined with enhanced post-training methodologies, displaying promise when applied to larger datasets in distillation processes. We have also observed that maintaining a smaller batch size is crucial for post-training on synthetic data to achieve commendable accuracy. This is attributed to the *Generalization Gap* (Keskar et al., 2016; Hoffer et al., 2017), which suggests that when there is a deficiency in the total training samples, the model's capacity to generalize to new, unseen data is not robust. Employing smaller batch sizes while training on the small-scale synthetic data allows models to explore the loss landscape more meticulously before converging to an optimal minimum.

3.3 Global-to-local Gradient Update via Curriculum

In SRe^{2}L (Yin et al., 2023) approach, the key of data synthesis revolves around utilizing the gradient information emanating from both the semantic class and the predictions of the pre-trained squeezing model, paired with BN distribution matching. Let $(\boldsymbol{x}, \boldsymbol{y})$ be an example $\boldsymbol{x}$ for optimization and its corresponding one-hot label $\boldsymbol{y}$ for the pre-trained squeezing model. Throughout the synthesis process, the squeezing model is frozen to recover the encoded information and ensure consistency and reliability in the generated data. Let $\mathcal{T}(\boldsymbol{x})$ be the target training distribution from which the data synthesis process should ultimately learn a function of desired trajectories, where $\mathcal{T}$ is a data transformation function to augment input samples to various levels of difficulties. Following Bengio et al. (2009), a weight $0 \leq W_s(x) \leq 1$ is defined and applied to example $\boldsymbol{x}$ at stage s in the curriculum sequence. The training distribution $D_s(x)$ is:

$$D_s(x) \propto W_s(x)\mathcal{T}(x) \quad \forall x \tag{4}$$

In our scenario, since the varying difficulties are governed by the data transformation function $\mathcal{T}$, we can straightforwardly employ $W_s(x) = 1$ across all stages. Consequently, the training distribution solely depends on $\mathcal{T}(x)$ and can be simplified as follows:

$$D(x) \propto \mathcal{T}(x) \quad \forall x \tag{5}$$

By integrating curriculum learning within the data synthesis phase, this procedure can be defined as:

Definition 1 (Curriculum Data Synthesis)**.** *In the data synthesis optimization, the corresponding sequence of distributions $D(x)$ will be a curriculum if there is an increment in the entropy of these distributions, i.e., the difficulty of the transformed input samples escalates and becomes increasingly challenging for the pre-trained model to predict as the training progresses.*

Thus, the key for our curriculum data synthesis becomes how to design $\mathcal{T}(x)$ across different training iterations. The following discusses several strategies to construct this in the curriculum scheme.

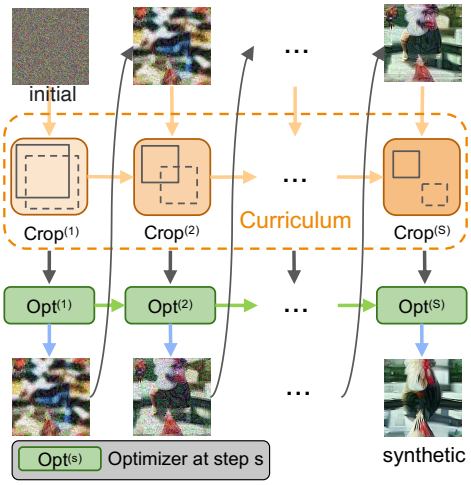

Figure 4: Global-to-local data synthesis.

Baseline: Constant Learning (CTL). This is the regular training method where all training examples are typically treated equally. Each sample from the training dataset has an equal chance of being transformed in a given batch, assuming no difficulty imbalance or biases across different training iterations.

CTL is straightforward to implement since we do not have to rank or organize examples based on difficulty. In practice, we use *RandomResizedCrop* to crop a small region via current crop ratio randomly sampled from a given interval [`min_crop`, `max_crop`] and then resize the cropped image to its original size, formulated as follows:

$$\boldsymbol{x}_{\mathcal{T}} \leftarrow \mathit{RandomResizedCrop}(\boldsymbol{x}_s,\ \texttt{min_crop} = \alpha_l,\ \texttt{max_crop} = \alpha_{\mathrm{u}}) \tag{6}$$

where α_l and α_{u} are the constant lower and upper bounds of crop scale.

Curriculum Learning (CL). As shown in Algorithm 1, in our CL, data samples are organized based on their difficulty. The difficulty level of the cropped region can be managed by defining the lower and upper scopes for the area ratio of the crop. This enables the assurance that specific crops of the image (small details or broader context) are included in the cropped region. For the difficulty adjustment, the rate at which more difficult examples are introduced and the criteria used to define difficulty are adjusted dynamically as predetermined using the following schedulers.

Step. Step scheduler reduces the minimal scale by a factor for every fixed or specified number of iterations, as shown in Figure 5 right.

Linear. Linear scheduler starts with a high initial value and decreases it linearly by a factor γ to a minimum value over the whole training.

Cosine. Cosine scheduler modulates the distribution according to the cosine function of the current iteration number, yielding a smoother and more gradual adjustment compared to step-based methods.

As shown in Figure 5, the factor distribution manages the difficulty level of crops with adjustable α_u and α_l for CTL and milestone for CL.

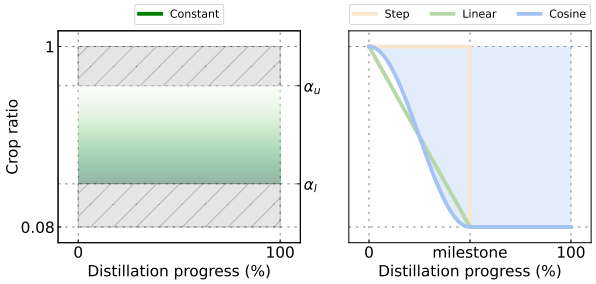

Figure 5: Crop ratio schedulers of prior CTL solution (left) and our *Global-to-local* (right) enabled by curriculum. The colored regions depict the random sampling intervals for the crop ratio value in each iteration under different schedulers.

Data Synthesis by Recovering and Relabeling. After receiving the transformed input $\boldsymbol{x}_{\mathcal{T}}$, we update it by aligning between the final classification label and intermediate Batch Normalization (BN) statistics, i.e., mean and variance from the original data. This stage forces the synthesized images to capture a shape of the original image distribution. The learning goal for this stage can be formulated as follows:

$$\boldsymbol{x}'_{\mathcal{T}} = \arg\min\ \ell\left(\phi_{\boldsymbol{\theta}}\left(\boldsymbol{x}_{\mathcal{T}}\right), \boldsymbol{y}\right) + \mathcal{R}_{\mathrm{reg}} \tag{7}$$

Algorithm 1: Our CDA via *RandomResizedCrop*

Input: squeezed model ϕ_θ, recovery iteration S, curriculum milestone T, target label $\boldsymbol{y}$, default lower and upper bounds of crop scale β_l and β_u in *RandomResizedCrop*, decay of lower scale bound γ
Output: synthetic image $\boldsymbol{x}$
Initialize: x_0 from a standard normal distribution
for step s from 0 to S-1 **do**
  if $s \leq T$ **then**
    $$\alpha \leftarrow \begin{cases} \beta_\mathrm{u} & \text{if } \texttt{step} \\ \beta_l + \gamma * (\beta_\mathrm{u} - s/T) & \text{if } \texttt{linear} \\ \beta_l + \gamma * (\beta_\mathrm{u} + \cos(\pi * s/T))/2 & \text{if } \texttt{cosine} \end{cases}$$
  else
    $\alpha \leftarrow \beta_l$
  end
  $\boldsymbol{x}_\mathcal{T} \leftarrow$ *RandomResizedCrop*$(\boldsymbol{x}_s, \texttt{min_crop} = \alpha, \texttt{max_crop} = \beta_\mathrm{u})$
  $\boldsymbol{x}'_\mathcal{T} \leftarrow \boldsymbol{x}_\mathcal{T}$ is optimized w.r.t ϕ_θ and $\boldsymbol{y}$ in Eq. 7.
  $\boldsymbol{x}_{s+1} \leftarrow$ *ReverseRandomResizedCrop*$(\boldsymbol{x}_s, \boldsymbol{x}'_\mathcal{T})$
end
return $\boldsymbol{x} \leftarrow \boldsymbol{x}_S$

where $\phi_{\boldsymbol{\theta}}$ is the pre-trained squeezing model and will be frozen in this stage. During synthesis, only the input crop area will be updated by the gradient from the objective. The entire training procedure is illustrated in Figure 4. After synthesizing the data, we follow the relabeling process in SRe^{2}L to generate soft labels (Shen & Xing, 2022) with the integration of the small batch size setting for post-training. $\mathcal{R}_\mathrm{reg}$ is the regularization term used in Yin et al. (2023), its detailed formulation using channel-wise mean and variance matching is:

$$\begin{aligned} \mathcal{R}_\mathrm{reg}(\boldsymbol{x}') &= \sum_k \|\mu_k(\boldsymbol{x}') - \mathbb{E}(\mu_k \mid \mathcal{D}_o)\|_2 + \sum_k \left\|\sigma_l^2(\boldsymbol{x}') - \mathbb{E}\left(\sigma_k^2 \mid \mathcal{D}_o\right)\right\|_2 \\ &\approx \sum_k \left\|\mu_k(\boldsymbol{x}') - \mathbf{BN}_k^\mathrm{RM}\right\|_2 + \sum_k \left\|\sigma_k^2(\boldsymbol{x}') - \mathbf{BN}_k^\mathrm{RV}\right\|_2 \end{aligned} \tag{8}$$

where k is the index of BN layer, $\mu_k(\boldsymbol{x}')$ and $\sigma_k^2(\boldsymbol{x}')$ are the channel-wise mean and variance in current batch data. $\mathbf{BN}_k^\mathrm{RM}$ and $\mathbf{BN}_k^\mathrm{RV}$ are mean and variance in the pre-trained model at k-th BN layer, which are globally counted.

Advantages of Global-to-local Synthesis. The proposed `CDA` enjoys several advantages: **(1)** Stabilized training: Curriculum synthesis can provide a more stable training process as it reduces drastic loss fluctuations that can occur when the learning procedure encounters a challenging sample early on. **(2)** Better generalization: By gradually increasing the difficulty, the synthetic data can potentially achieve better generalization on diverse model architectures in post-training. It reduces the chance of the synthesis getting stuck in poor local minima early in the training process. **(3)** Avoid overfitting: By ensuring that the synthetic data is well-tuned on simpler examples before encountering outliers or more challenging data, there is a potential to reduce overfitting.

4 Experiments

4.1 Datasets and Implementation Details

We verify the effectiveness of our approach on small-scale CIFAR-100 and various ImageNet scale datasets, including Tiny-ImageNet (Le & Yang, 2015), ImageNet-1K (Deng et al., 2009), and ImageNet-21K (Ridnik et al., 2021). For evaluation, we train models from scratch on synthetic distilled datasets and report the Top-1 accuracy on real validation datasets. Default lower and upper bounds of crop scales β_l and β_u are 0.08 and 1.0, respectively. The decay γ is 0.92. In Curriculum Learning (CL) settings, the actual lower bound is dynamically adjusted to control difficulty, whereas the upper bound is fixed to the default value of 1.0 to

Table 1: Comparison with state-of-the-art methods on various datasets.

Dataset	CIFAR-100		Tiny-ImageNet			ImageNet-1K				ImageNet-21K	
IPC	10	50	10	50	100	10	50	100	200	10	20
Ratio (%)	2	10	2	10	20	0.8	4	8	16	0.8	1.6
DM	29.7±0.3	43.6±0.4	12.9±0.4	24.1±0.3	-	5.7±0.1	11.4±0.9	-	-	-	-
DSA	32.3±0.3	42.8±0.4	-	-	-	-	-	-	-	-	-
FRePo	42.5±0.2	44.3±0.2	25.4±0.2	-	-	-	-	-	-	-	-
MTT	39.7±0.4	47.7±0.2	23.2±0.2	28.0±0.3	-	-	-	-	-	-	-
DataDAM	34.8±0.5	49.4±0.3	18.7±0.3	28.7±0.3	-	6.3±0.0	15.5±0.2	-	-	-	-
TESLA	41.7±0.3	47.9±0.3	-	-	-	17.8±1.3	27.9±1.2	-	-	-	-
DATM	47.2±0.4	55.0±0.2	**31.1±0.3**	39.7±0.3	-	-	-	-	-	-	-
Full Dataset[1]	*79.1*		*61.2*			*69.8*				*38.5*	
SRe^{2}L	23.5±0.8	51.4±0.8	17.7±0.7*	41.1±0.4	49.7±0.3	21.3±0.6*	46.8±0.2	52.8±0.4	57.0±0.3	18.5±0.2*	21.8±0.1*
CDA (Ours)	**49.5±0.6**	**64.0±0.5**	21.3±0.3	**48.7±0.1**	**53.2±0.1**	**33.5±0.3**	**53.5±0.3**	**58.0±0.2**	**63.3±0.2**	**22.6±0.2**	**26.4±0.1**

* Replicated experiment results are marked with *, while the other baseline results are referenced from original papers.
[1] The full dataset results refer to Top-1 val accuracy achieved by a ResNet-18 model trained on the full dataset, the architecture is the same as SRe^{2}L and our `CDA`.

ensure there is a probability of cropping and optimizing the entire image in any progress. More details are provided in the Appendix B.

4.2 CIFAR-100

Result comparisons with baseline methods, including DM (Zhao & Bilen, 2023), DSA (Zhao & Bilen, 2021), FRePo (Zhou et al., 2022), MTT (Cazenavette et al., 2022b), DataDAM (Sajedi et al., 2023), TESLA (Cui et al., 2023), DATM (Guo et al., 2024), and SRe^{2}L (Yin et al., 2023) on CIFAR-100 are presented in Table 1. Our model is trained with an 800ep budget. It can be observed that our `CDA` validation accuracy outperforms all baselines under 10 and 50 IPC. And our reported results have the potential to be further improved as training budgets increase. Overall, our `CDA` method is also applicable to small-scale dataset distillation.

4.3 Tiny-ImageNet

Results on the Tiny-ImageNet dataset are detailed in the second group of Table 1 and the first group of Table 3. Our `CDA` outperforms all baselines except DATM under 10 IPC. Compared to SRe^{2}L, our `CDA` achieves average improvements of 7.7% and 3.4% under IPC 50 and IPC 100 settings across ResNet-{18, 50, 101} validation models, respectively. Importantly, `CDA` stands as the inaugural approach to diminish the Top-1 accuracy performance disparity to less than 10% between the distilled dataset employing IPC 100 and the full Tiny-ImageNet, signifying a breakthrough on this dataset.

4.4 ImageNet-1K

Table 2: Constant learning result. α_l and α_u stand for the `min_crop` and `max_crop` parameters in *RandomResizedCrop*. ‡ represents the results from SRe^{2}L implementation but following the setting in the table.

Constant learning type $\setminus$ α	0.08	0.2	0.4	0.6	0.8	1.0
Easy ($\alpha_l = \alpha, \alpha_u = \beta_u$)	44.90‡	**47.88**	46.34	45.35	43.48	41.30
Hard ($\alpha_l = \beta_l, \alpha_u = \alpha$)	22.99	34.75	42.76	44.61	**45.76**	44.90‡

Constant Learning (CTL). We leverage a ResNet-18 and employ synthesized data with 1K recovery iterations. As observed in Table 2, the results for exceedingly straightforward or challenging scenarios fall below the reproduced SRe^{2}L baseline accuracy of 44.90%, especially when $\alpha \geq 0.8$ in *easy* and $\alpha \leq 0.4$ in *hard* type. Thus, the results presented in Table 2 suggest that adopting a larger cropped range assists in circumventing extreme scenarios, whether easy or hard, culminating in enhanced performance. A noteworthy observation is the crucial role of appropriate lower and upper bounds for constant learning in boosting validation accuracy. This highlights the importance of employing curriculum data augmentation strategies in data synthesis.

Table 3: Comparison with baseline on various datasets.

Dataset	IPC	ResNet-18		ResNet-50		ResNet-101	
		SRe^{2}L	Ours	SRe^{2}L	Ours	SRe^{2}L	Ours
Tiny-IN	50	41.1	$48.7^{\uparrow 7.6}$	42.2	$49.7^{\uparrow 7.5}$	42.5	$50.6^{\uparrow 8.1}$
	100	49.7	$53.2^{\uparrow 3.5}$	51.2	$54.4^{\uparrow 3.2}$	51.5	$55.0^{\uparrow 3.5}$
IN-1K	50	46.8	$53.5^{\uparrow 6.7}$	55.6	$61.3^{\uparrow 5.7}$	57.6	$61.6^{\uparrow 4.0}$
	100	52.8	$58.0^{\uparrow 5.2}$	61.0	$65.1^{\uparrow 4.1}$	62.8	$65.9^{\uparrow 3.1}$
	200	57.0	$63.3^{\uparrow 6.3}$	64.6	$67.6^{\uparrow 3.0}$	65.9	$68.4^{\uparrow 2.5}$
IN-21K	10	18.5	$22.6^{\uparrow 4.1}$	27.4	$32.4^{\uparrow 5.0}$	27.3	$34.2^{\uparrow 6.9}$
	20	21.8	$26.4^{\uparrow 4.6}$	31.3	$35.3^{\uparrow 4.0}$	33.2	$36.1^{\uparrow 2.9}$

Curriculum Learning (CL). We follow the recovery recipe of SRe^{2}L's best result for 4K recovery iterations. As illustrated in Table 1 and the second group of Table 3, when compared to the strong baseline SRe^{2}L, `CDA` enhances the validation accuracy, exhibiting average margins of 6.1%, 4.3%, and 3.2% on ResNet-{18, 50, 101} across varying IPC settings. Furthermore, as shown in Figure 1, the results achieve with our `CDA` utilizing merely 1K recovery iterations surpass those of SRe^{2}L encompassing the entire 4K iterations. These results substantiate the efficacy and effectiveness of applying `CDA` in large-scale dataset distillation.

4.5 ImageNet-21K

Pre-training Results. Table 18 of the Appendix presents the accuracy for ResNet-18 and ResNet-50 on ImageNet-21K-P, considering varying initial weight configurations. Models pre-trained by us and initialized with ImageNet-1K weight exhibit commendable accuracy, showing a 2.0% improvement, while models initialized randomly achieve marginally superior accuracy. We utilize these pre-trained models to recover ImageNet-21K data and to assign labels to the synthetic images generated. An intriguing observation is the heightened difficulty in data recovering from pre-trained models that are initialized randomly compared to those initialized with ImageNet-1K weight. Thus, our experiments employ `CDA` specifically on pre-trained models that are initialized with ImageNet-1K weight.

Validation Results. As illustrated in Table 1 and the final group of Table 3, we perform validation experiments on the distilled ImageNet-21K employing IPC 10 and 20. This yields an extreme compression ratio of 100× and 50×. When applying IPC 10, i.e., the models are trained utilizing a distilled dataset that is a mere 1% of the full dataset. Remarkably, validation accuracy surpasses 20% and 30% on ResNet-18 and ResNet-{50, 101}, respectively. Compared to reproduced SRe^{2}L on ImageNet-21K, our approach attains an elevation of 5.3% on average under IPC 10/20. This not only highlights the efficacy of our approach in maintaining dataset essence despite high compression but also showcases the potential advancements in accuracy over existing methods.

4.6 Ablations

Curriculum Scheduler. To schedule the global-to-local learning, we present three distinct types of curriculum schedulers, *step*, *linear*, and *cosine* to manipulate the lower bounds on data cropped augmentation. As illustrated in Figure 5, the dataset distillation progress is divided into two phases by a milestone. It is observed that both *linear* and *cosine* with continuous decay manifest robustness across diverse milestone configurations and reveal a trend of enhancing accuracy performance when the milestone is met at a later phase, as shown in Figure 6. Moreover, *cosine* marginally outperforms *linear* in terms of accuracy towards the end. Consequently, we choose to implement the *cosine* scheduler, assigning a milestone percentage of 1.0, to modulate the minimum crop ratio adhering to the principles of curriculum learning throughout the progression of synthesis.

Batch Size in Post-training. We perform an ablation study to assess the influence of utilizing smaller batch sizes on the generalization performance of models when the synthetic data is limited. We report results on the distilled ImageNet-21K from ResNet-18. In Table 4, a

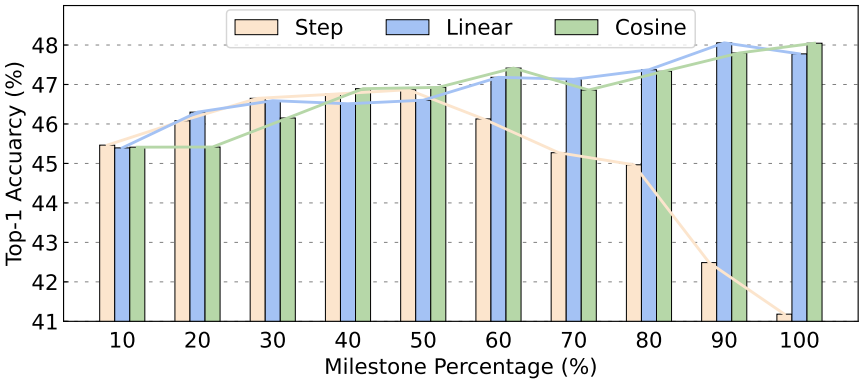

Figure 6: Ablation study on three different schedulers with varied milestone settings.

rise in validation accuracy is observed as batch size reduces, peaking at 16. This suggests that smaller batch sizes enhance performance on small-scale synthetic datasets. However, this leads to more frequent data loading and lower GPU utilization in our case, extending training times. To balance training time with performance, we chose a batch size of 32 for our experiments.

4.7 Analysis

Cross-Model Generalization. The challenge of ensuring distilled datasets generalize effectively across models unseen during the recovery phase remains significant, as in prior approaches (Zhao et al., 2020; Cazenavette et al., 2022a), synthetic images were optimized to overfit the recovery model. In the first group of Table 5, we deploy our ImageNet-1K distilled datasets to train various validation models, and we attain over 60% Top-1 accuracy with most of these models. Additionally, our performance in Top-1 accuracy surpasses that of SRe^{2}L across all validation models spanning various architectures. Although DeiT-Tiny is not validated with a comparable Top-1 accuracy to other CNN models due to the ViT's inherent characteristic requiring more training data, `CDA` achieves double cross-model generation performance on the DeiT-Tiny validation model, compared with SRe^{2}L. More validation models on distilled ImageNet-1K are included in Table 16 of the Appendix. The second group of Table 5 supports further empirical substantiation of the `CDA`'s efficacy in the distillation of large-scale ImageNet-21K datasets. The results demonstrate that the `CDA`'s distilled datasets exhibit reduced dependency on specific recovery models, thereby further alleviating the overfitting optimization issues.

Table 4: Ablation on batch size in validation.

Batch Size	Acc. (%)
128	20.79
64	21.85
32	22.54
16	**22.75**
8	22.41

Table 5: Cross-model generation on distilled ImageNet-1K with 50 IPC and ImageNet-21K with 20 IPC.

Dataset	Method	Validation Model						
		R18	R50	R101	DenseNet-121	RegNet-Y-8GF	ConvNeXt-Tiny	DeiT-Tiny
IN-1K	SRe^{2}L	46.80	55.60	57.60	49.74	60.34	53.53	15.41
	`CDA` (ours)	**53.45**	**61.26**	**61.57**	**57.35**	**63.22**	**62.58**	**31.95**
IN-21K	SRe^{2}L	21.83	31.26	33.24	24.66	34.22	34.95	15.76
	`CDA` (ours)	**26.42**	**35.32**	**36.12**	**28.66**	**36.13**	**36.31**	**18.56**

Impact of Curriculum. To study the curriculum's advantage on synthetic image characteristics, we evaluate the Top-1 accuracy on `CDA`, SRe^{2}L and real ImageNet-1K training set, using a åmean of random 10-crop and global images. We employ PyTorch's pre-trained MobileNet-V2 to classify these images. As shown in Table 6, `CDA` images closely resemble real ImageNet images in prediction accuracies, better than SRe^{2}L. Consequently, curriculum data augmentation im-

Table 6: Classification accuracy using MobileNet-V2.

Top-1 (%)	Dataset		
	SRe^{2}L	`CDA` (ours)	Real
global	79.34	81.25	82.16
cropped	87.48	82.44	72.73

proves global image prediction and reduces bias and overfitting post-training on simpler, cropped images of SRe^{2}L.

Visualization and Discussion. Figure 7 provides a comparative visualization of the gradient synthetic images at recovery steps of {100, 500, 1K, 2K} to illustrate the differences between SRe^{2}L and `CDA` within the dataset distillation process. SRe^{2}L images in the upper line exhibit a significant amount of noise, indicating a slow recovery progression in the early recovery stage. On the contrary, due to the mostly entire image optimization in the early stage, `CDA` images in the lower line can establish the layout of the entire image and reduce noise rapidly. And the final synthetic images contain more visual information directly related to the target class *Plant*. Therefore, the comparison highlights `CDA`'s ability to synthesize images with enhanced visual coherence to the target class, offering a more efficient recovery process. More visualizations are provided in Appendix D.

Figure 7: Synthetic ImageNet-21K images (*Plant*).

Synthesis Cost. We highlight that there is no additional synthesis cost incurred in our `CDA` to SRe^{2}L (Yin et al., 2023) under the same recovery iteration setting. Specifically, for ImageNet-1K, it takes about 29 hours to generate the distilled ImageNet-1K with 50 IPC on a single A100 (40G) GPU and the peak GPU memory utilization is 6.7GB. For ImageNet-21K, it takes 11 hours to generate ImageNet-21K images per IPC on a single RTX 4090 GPU and the peak GPU memory utilization is 15GB. In our experiment, it takes about 55 hours to generate the entire distilled ImageNet-21K with 20 IPC on 4× RTX 4090 GPUs in total.

4.8 Application: Continual Learning

The distilled datasets, comprising high-semantic images, possess a boosted representation capacity compared to the original datasets. This attribute can be strategically harnessed to combat catastrophic forgetting in continual learning. We have further validated the effectiveness of our introduced `CDA` synthesis within various continual learning scenarios. Following the setting introduced in SRe^{2}L (Yin et al., 2023), we conducted 5-step and 10-step class-incremental experiments on Tiny-ImageNet, aligning our results against the baseline SRe^{2}L and a randomly selected subset on Tiny-ImageNet for comparative analysis. As illustrated in Figure 8, our `CDA` distilled dataset notably surpasses SRe^{2}L, exhibiting an average advantage of 3.8% and 4.5% on 5-step and 10-step class-incremental learning assignments respectively. This demonstrates the substantial benefits inherent in the generation of `CDA`, particularly in mitigating the complexities associated with continual learning.

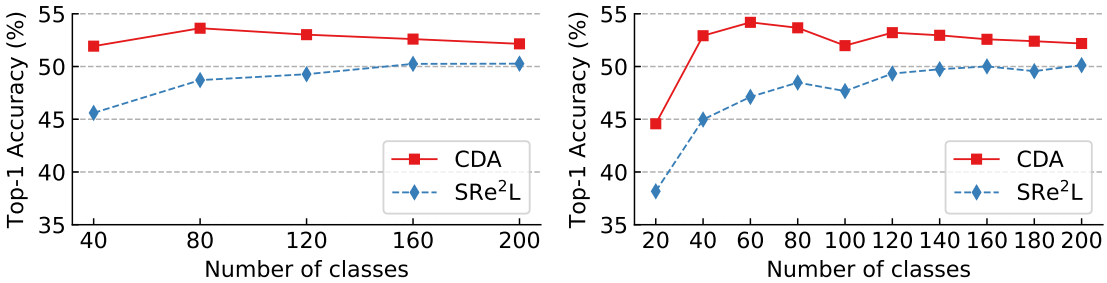

Figure 8: 5/10-step class-incremental learning on Tiny-IN.

5 Conclusion

We presented a new framework focused on *global-to-local* gradient refinement through curriculum data synthesis for large-scale dataset distillation. Our approach involves a practical paradigm with detailed pertaining for compressing knowledge, data synthesis for recovery, and post-training recipes. The proposed approach enables the distillation of ImageNet-21K to 50× smaller while maintaining competitive accuracy levels. In

regular benchmarks, such as ImageNet-1K and CIFAR-100, our approach also demonstrated superior performance, surpassing prior state-of-the-art methods by substantial margins. We further show the capability of our synthetic data on downstream tasks of cross-model generalization and continual learning. With the recent substantial growth in the size of both models and datasets, the critical need for dataset distillation on large-scale datasets and models has become increasingly prominent and urgent. Our future work will focus on distilling more modalities like language and speech.

References

Ali Abbasi, Ashkan Shahbazi, Hamed Pirsiavash, and Soheil Kolouri. One category one prompt: Dataset distillation using diffusion models. *arXiv preprint arXiv:2403.07142*, 2024.

Yoshua Bengio, Jérôme Louradour, Ronan Collobert, and Jason Weston. Curriculum learning. In *Proceedings of the 26th annual international conference on machine learning*, pp. 41–48, 2009.

Tom Brown, Benjamin Mann, Nick Ryder, Melanie Subbiah, Jared D Kaplan, Prafulla Dhariwal, Arvind Neelakantan, Pranav Shyam, Girish Sastry, Amanda Askell, et al. Language models are few-shot learners. *Advances in neural information processing systems*, 33:1877–1901, 2020.

George Cazenavette, Tongzhou Wang, Antonio Torralba, Alexei A Efros, and Jun-Yan Zhu. Dataset distillation by matching training trajectories. In *Proceedings of the IEEE/CVF Conference on Computer Vision and Pattern Recognition*, pp. 4750–4759, 2022a.

George Cazenavette, Tongzhou Wang, Antonio Torralba, Alexei A. Efros, and Jun-Yan Zhu. Wearable imagenet: Synthesizing tileable textures via dataset distillation. In *Proceedings of the IEEE/CVF Conference on Computer Vision and Pattern Recognition Workshops*, 2022b.

George Cazenavette, Tongzhou Wang, Antonio Torralba, Alexei A Efros, and Jun-Yan Zhu. Generalizing dataset distillation via deep generative prior. In *Proceedings of the IEEE/CVF Conference on Computer Vision and Pattern Recognition*, pp. 3739–3748, 2023.

Mingyang Chen, Bo Huang, Junda Lu, Bing Li, Yi Wang, Minhao Cheng, and Wei Wang. Dataset distillation via adversarial prediction matching. *arXiv preprint arXiv:2312.08912*, 2023.

Ekin D Cubuk, Barret Zoph, Jonathon Shlens, and Quoc V Le. Randaugment: Practical automated data augmentation with a reduced search space. In *Proceedings of the IEEE/CVF conference on computer vision and pattern recognition workshops*, pp. 702–703, 2020.

Justin Cui, Ruochen Wang, Si Si, and Cho-Jui Hsieh. Scaling up dataset distillation to imagenet-1k with constant memory. In *International Conference on Machine Learning*, pp. 6565–6590. PMLR, 2023.

Justin Cui, Ruochen Wang, Yuanhao Xiong, and Cho-Jui Hsieh. Ameliorate spurious correlations in dataset condensation. In *Forty-first International Conference on Machine Learning*, 2024.

Mostafa Dehghani, Josip Djolonga, Basil Mustafa, Piotr Padlewski, Jonathan Heek, Justin Gilmer, Andreas Peter Steiner, Mathilde Caron, Robert Geirhos, Ibrahim Alabdulmohsin, et al. Scaling vision transformers to 22 billion parameters. In *International Conference on Machine Learning*, pp. 7480–7512. PMLR, 2023.

Jia Deng, Wei Dong, Richard Socher, Li-Jia Li, Kai Li, and Li Fei-Fei. Imagenet: A large-scale hierarchical image database. In *2009 IEEE conference on computer vision and pattern recognition*, pp. 248–255. Ieee, 2009.

Zhiwei Deng and Olga Russakovsky. Remember the past: Distilling datasets into addressable memories for neural networks. *arXiv preprint arXiv:2206.02916*, 2022.

Terrance DeVries and Graham W Taylor. Improved regularization of convolutional neural networks with cutout. *arXiv preprint arXiv:1708.04552*, 2017.

Alexey Dosovitskiy, Lucas Beyer, Alexander Kolesnikov, Dirk Weissenborn, Xiaohua Zhai, Thomas Unterthiner, Mostafa Dehghani, Matthias Minderer, Georg Heigold, Sylvain Gelly, et al. An image is worth 16x16 words: Transformers for image recognition at scale. *arXiv preprint arXiv:2010.11929*, 2020.

Jiawei Du, Qin Shi, and Joey Tianyi Zhou. Sequential subset matching for dataset distillation. *Advances in Neural Information Processing Systems*, 36, 2023.

Jianyang Gu, Saeed Vahidian, Vyacheslav Kungurtsev, Haonan Wang, Wei Jiang, Yang You, and Yiran Chen. Efficient dataset distillation via minimax diffusion. *arXiv preprint arXiv:2311.15529*, 2023.

Ziyao Guo, Kai Wang, George Cazenavette, Hui Li, Kaipeng Zhang, and Yang You. Towards lossless dataset distillation via difficulty-aligned trajectory matching. In *The Twelfth International Conference on Learning Representations*, 2024.

Kaiming He, Xiangyu Zhang, Shaoqing Ren, and Jian Sun. Deep residual learning for image recognition. In *Proceedings of the IEEE conference on computer vision and pattern recognition*, pp. 770–778, 2016.

Kaiming He, Haoqi Fan, Yuxin Wu, Saining Xie, and Ross Girshick. Momentum contrast for unsupervised visual representation learning. In *Proceedings of the IEEE/CVF conference on computer vision and pattern recognition*, pp. 9729–9738, 2020.

Yang He, Lingao Xiao, Joey Tianyi Zhou, and Ivor Tsang. Multisize dataset condensation. *ICLR*, 2024.

Elad Hoffer, Itay Hubara, and Daniel Soudry. Train longer, generalize better: closing the generalization gap in large batch training of neural networks. *Advances in neural information processing systems*, 30, 2017.

Gao Huang, Zhuang Liu, Laurens Van Der Maaten, and Kilian Q Weinberger. Densely connected convolutional networks. In *Proceedings of the IEEE conference on computer vision and pattern recognition*, pp. 4700–4708, 2017.

Nitish Shirish Keskar, Dheevatsa Mudigere, Jorge Nocedal, Mikhail Smelyanskiy, and Ping Tak Peter Tang. On large-batch training for deep learning: Generalization gap and sharp minima. *arXiv preprint arXiv:1609.04836*, 2016.

Jang-Hyun Kim, Jinuk Kim, Seong Joon Oh, Sangdoo Yun, Hwanjun Song, Joonhyun Jeong, Jung-Woo Ha, and Hyun Oh Song. Dataset condensation via efficient synthetic-data parameterization. In *International Conference on Machine Learning*, pp. 11102–11118. PMLR, 2022a.

Jang-Hyun Kim, Jinuk Kim, Seong Joon Oh, Sangdoo Yun, Hwanjun Song, Joonhyun Jeong, Jung-Woo Ha, and Hyun Oh Song. Dataset condensation via efficient synthetic-data parameterization. In *Proceedings of the 39th International Conference on Machine Learning*, 2022b.

Ya Le and Xuan Yang. Tiny imagenet visual recognition challenge. *CS 231N*, 7(7):3, 2015.

Saehyung Lee, Sanghyuk Chun, Sangwon Jung, Sangdoo Yun, and Sungroh Yoon. Dataset condensation with contrastive signals. In *International Conference on Machine Learning*, pp. 12352–12364. PMLR, 2022.

Haoyang Liu, Tiancheng Xing, Luwei Li, Vibhu Dalal, Jingrui He, and Haohan Wang. Dataset distillation via the wasserstein metric. *arXiv preprint arXiv:2311.18531*, 2023.

Songhua Liu, Kai Wang, Xingyi Yang, Jingwen Ye, and Xinchao Wang. Dataset distillation via factorization. *Advances in Neural Information Processing Systems*, 35:1100–1113, 2022a.

Zhuang Liu, Hanzi Mao, Chao-Yuan Wu, Christoph Feichtenhofer, Trevor Darrell, and Saining Xie. A convnet for the 2020s. In *Proceedings of the IEEE/CVF conference on computer vision and pattern recognition*, pp. 11976–11986, 2022b.

Noel Loo, Ramin Hasani, Alexander Amini, and Daniela Rus. Efficient dataset distillation using random feature approximation. *arXiv preprint arXiv:2210.12067*, 2022.

Zhiheng Ma, Anjia Cao, Funing Yang, and Xing Wei. Curriculum dataset distillation. *arXiv preprint arXiv:2405.09150*, 2024.

Aru Maekawa, Naoki Kobayashi, Kotaro Funakoshi, and Manabu Okumura. Dataset distillation with attention labels for fine-tuning bert. In *Proceedings of the 61st Annual Meeting of the Association for Computational Linguistics (Volume 2: Short Papers)*, pp. 119–127, 2023.

Timothy Nguyen, Roman Novak, Lechao Xiao, and Jaehoon Lee. Dataset distillation with infinitely wide convolutional networks. *Advances in Neural Information Processing Systems*, 34:5186–5198, 2021.

OpenAI. Gpt-4 technical report, 2023.

Tian Qin, Zhiwei Deng, and David Alvarez-Melis. Distributional dataset distillation with subtask decomposition. *arXiv preprint arXiv:2403.00999*, 2024.

Ilija Radosavovic, Raj Prateek Kosaraju, Ross Girshick, Kaiming He, and Piotr Dollár. Designing network design spaces. In *Proceedings of the IEEE/CVF conference on computer vision and pattern recognition*, pp. 10428–10436, 2020.

Tal Ridnik, Emanuel Ben-Baruch, Asaf Noy, and Lihi Zelnik-Manor. Imagenet-21k pretraining for the masses. *arXiv preprint arXiv:2104.10972*, 2021.

Robin Rombach, Andreas Blattmann, Dominik Lorenz, Patrick Esser, and Björn Ommer. High-resolution image synthesis with latent diffusion models. In *Proceedings of the IEEE/CVF conference on computer vision and pattern recognition*, pp. 10684–10695, 2022.

Ahmad Sajedi, Samir Khaki, Ehsan Amjadian, Lucy Z. Liu, Yuri A. Lawryshyn, and Konstantinos N. Plataniotis. Datadam: Efficient dataset distillation with attention matching. In *Proceedings of the IEEE/CVF International Conference on Computer Vision (ICCV)*, pp. 17097–17107, October 2023.

Xinyi Shang, Peng Sun, and Tao Lin. Gift: Unlocking full potential of labels in distilled dataset at near-zero cost. *arXiv preprint arXiv:2405.14736*, 2024.

Shitong Shao, Zeyuan Yin, Muxin Zhou, Xindong Zhang, and Zhiqiang Shen. Generalized large-scale data condensation via various backbone and statistical matching. *CVPR*, 2024a.

Shitong Shao, Zikai Zhou, Huanran Chen, and Zhiqiang Shen. Elucidating the design space of dataset condensation. *arXiv preprint arXiv:2404.13733*, 2024b.

Zhiqiang Shen and Eric Xing. A fast knowledge distillation framework for visual recognition. In *European Conference on Computer Vision*, pp. 673–690. Springer, 2022.

Donghyeok Shin, Seungjae Shin, and Il-Chul Moon. Frequency domain-based dataset distillation. *Advances in Neural Information Processing Systems*, 36, 2024.

Ilia Sucholutsky and Matthias Schonlau. Soft-label dataset distillation and text dataset distillation. In *2021 International Joint Conference on Neural Networks (IJCNN)*, pp. 1–8. IEEE, 2021.

Peng Sun, Bei Shi, Daiwei Yu, and Tao Lin. On the diversity and realism of distilled dataset: An efficient dataset distillation paradigm. *arXiv preprint arXiv:2312.03526*, 2023.

Peng Sun, Bei Shi, Daiwei Yu, and Tao Lin. On the diversity and realism of distilled dataset: An efficient dataset distillation paradigm. In *Proceedings of the IEEE/CVF Conference on Computer Vision and Pattern Recognition (CVPR)*, 2024.

Hugo Touvron, Matthieu Cord, Matthijs Douze, Francisco Massa, Alexandre Sablayrolles, and Hervé Jégou. Training data-efficient image transformers & distillation through attention. In *International conference on machine learning*, pp. 10347–10357. PMLR, 2021.

Kai Wang, Bo Zhao, Xiangyu Peng, Zheng Zhu, Shuo Yang, Shuo Wang, Guan Huang, Hakan Bilen, Xinchao Wang, and Yang You. Cafe: Learning to condense dataset by aligning features. In *Proceedings of the IEEE/CVF Conference on Computer Vision and Pattern Recognition (CVPR)*, 2022.

Tongzhou Wang, Jun-Yan Zhu, Antonio Torralba, and Alexei A Efros. Dataset distillation. *arXiv preprint arXiv:1811.10959*, 2018.

Tongzhou Wang, Jun-Yan Zhu, Antonio Torralba, and Alexei A. Efros. Dataset distillation, 2020.

Yifan Wu, Jiawei Du, Ping Liu, Yuewei Lin, Wenqing Cheng, and Wei Xu. Dd-robustbench: An adversarial robustness benchmark for dataset distillation. *arXiv preprint arXiv:2403.13322*, 2024.

Eric Xue, Yijiang Li, Haoyang Liu, Yifan Shen, and Haohan Wang. Towards adversarially robust dataset distillation by curvature regularization. *arXiv preprint arXiv:2403.10045*, 2024.

Zeyuan Yin, Eric Xing, and Zhiqiang Shen. Squeeze, recover and relabel: Dataset condensation at imagenet scale from a new perspective. In *NeurIPS*, 2023.

Bo Zhao and Hakan Bilen. Dataset condensation with differentiable siamese augmentation. In *International Conference on Machine Learning*, pp. 12674–12685. PMLR, 2021.

Bo Zhao and Hakan Bilen. Dataset condensation with distribution matching. In *IEEE/CVF Winter Conference on Applications of Computer Vision, WACV 2023, Waikoloa, HI, USA, January 2-7, 2023*, 2023.

Bo Zhao, Konda Reddy Mopuri, and Hakan Bilen. Dataset condensation with gradient matching. *arXiv preprint arXiv:2006.05929*, 2020.

Binglin Zhou, Linhao Zhong, and Wentao Chen. Improve cross-architecture generalization on dataset distillation. *arXiv preprint arXiv:2402.13007*, 2024a.

Muxin Zhou, Zeyuan Yin, Shitong Shao, and Zhiqiang Shen. Self-supervised dataset distillation: A good compression is all you need. *arXiv preprint arXiv:2404.07976*, 2024b.

Yongchao Zhou, Ehsan Nezhadarya, and Jimmy Ba. Dataset distillation using neural feature regression. *Advances in Neural Information Processing Systems*, 35:9813–9827, 2022.

Appendix

A Datasets Details

We conduct experiments on three ImageNet scale datasets, Tiny-ImageNet (Le & Yang, 2015), ImageNet-1K (Deng et al., 2009), and ImageNet-21K (Ridnik et al., 2021). The dataset details are as follows:

- CIFAR-100 dataset composes 500 training images per class, each with a resolution of 32×32 pixels, across 100 classes.
- Tiny-ImageNet dataset is derived from ImageNet-1K and consists of 200 classes. Within each category, there are 500 images with a uniform 64×64 resolution.
- ImageNet-1K dataset comprises 1,000 classes and 1,281,167 images in total. We resize all images into standard 224×224 resolution during the data loading stage.
- The original ImageNet-21K dataset is an extensive visual recognition dataset containing 21,841 classes and 14,197,122 images. We use ImageNet-21K-P (Ridnik et al., 2021) which utilizes data processing to remove infrequent classes and resize all images to 224×224 resolution. After data processing, ImageNet-21K-P dataset consists of 10,450 classes and 11,060,223 images.

B Implementation Details

B.1 CIFAR-100

Hyper-parameter Setting. We train a modified ResNet-18 model (He et al., 2020) on CIFAR-100 training data with a Top-1 accuracy of 79.1% using the parameter setting in Table 7a. The well-trained model serves as the recovery model under the recovery setting in Table 7b.

Table 7: Hyper-parameter settings on CIFAR-100.

(a) Squeezing/validation setting.

config	value
optimizer	SGD
base learning rate	0.1
momentum	0.9
weight decay	5e-4
batch size	128 (squeeze) / 8 (val)
learning rate schedule	cosine decay
training epoch	200 (squeeze) / 800 (val)
augmentation	RandomResizedCrop

(b) Recovery setting.

config	value
α_{BN}	0.01
optimizer	Adam
base learning rate	0.25
momentum	β_1, $\beta_2 = 0.5, 0.9$
batch size	100
learning rate schedule	cosine decay
recovery iteration	1,000
augmentation	RandomResizedCrop

Due to the low resolution of CIFAR images, the default lower bound β_l needs to be raised from 0.08 (ImageNet setting) to a higher reasonable value in order to avoid the training inefficiency caused by extremely small cropped areas with little information. Thus, we conducted the ablation to select the optimal value for the default lower bound β_l in RandomResizedCrop operations in Table 8. We choose 0.4 as the default lower bound β_l in Algorithm 1 to exhibit the best distillation performance on CIFAR-100. We adopt a small batch size value of 8 and extend the training budgets in the following validation stage, which aligns with the strong training recipe on inadequate datasets.

Table 8: Ablation on the lower bound β_l setting in distilling CIFAR-100.

default lower bound β_l	0.08	0.2	0.4	0.6	0.8	1.0
validation accuracy (800ep) (%)	58.5	62.14	**64.0**	63.36	61.65	54.43

B.2 Tiny-ImageNet

Hyper-parameter Setting. We train a modified ResNet-18 model (He et al., 2020) on Tiny-ImageNet training data with the parameter setting in Table 9a and use the well-trained ResNet-18 model with a Top-1 accuracy of 61.2% as a recovery model for `CDA`. The recovery setting is provided in Table 9b.

Table 9: Hyper-parameter settings on Tiny-ImageNet.

(a) Squeezing/validation setting.

config	value
optimizer	SGD
base learning rate	0.2
momentum	0.9
weight decay	1e-4
batch size	256 (squeeze) / 64 (val)
learning rate schedule	cosine decay
training epoch	50 (squeeze) / 100 (val)
augmentation	RandomResizedCrop

(b) Recovery setting.

config	value
α_{BN}	1.0
optimizer	Adam
base learning rate	0.1
momentum	β_1, $\beta_2 = 0.5, 0.9$
batch size	100
learning rate schedule	cosine decay
recovery iteration	4,000
augmentation	RandomResizedCrop

Small IPC Setting Comparison. Table 10 presents the result comparison among our `CDA`, DM (Zhao & Bilen, 2023) and MTT (Cazenavette et al., 2022b). Consider that our approach is a decoupled process of dataset compression followed by recovery through gradient updating. It is well-suited to large-scale datasets but less so for small IPC values. As anticipated, there is no advantage when IPC value is extremely low, such as IPC = 1. However, when the IPC is increased slightly, our method demonstrates considerable benefits on accuracy over other counterparts. Furthermore, we emphasize that our approach yields substantial improvements when afforded a larger training budget, i.e., more training epochs.

Table 10: Comparison with baseline methods on Tiny-ImageNet.

Tiny-ImageNet IPC	DM	MTT	`CDA` (200ep)	`CDA` (400ep)	`CDA` (800ep)
1	3.9	**8.8**	2.38 ± 0.08	2.82 ± 0.06	3.29 ± 0.26
10	12.9	23.2	30.41 ± 1.53	37.41 ± 0.02	**43.04 ± 0.26**
20	–	–	43.93 ± 0.20	47.76 ± 0.19	**50.46 ± 0.14**
50	24.1	28.0	50.26 ± 0.09	51.52 ± 0.17	**55.50 ± 0.18**

Continual Learning. We adhere to the continual learning codebase outlined in Zhao et al. (2020) and validate provided SRe^{2}L and our `CDA` distilled Tiny-ImageNet dataset under IPC 100 as illustrated in Figure 8. Detailed values are presented in the Table 11 and Table 12.

Table 11: 5-step class-incremental learning on Tiny-ImageNet. This complements details in the left subfigure of Figure 8.

# class	40	80	120	160	200
SRe^{2}L	45.60	48.71	49.27	50.25	50.27
`CDA` (ours)	51.93	53.63	53.02	52.60	52.15

Table 12: 10-step class-incremental learning on Tiny-ImageNet. This complements details in the right subfigure of Figure 8.

# class	20	40	60	80	100	120	140	160	180	200
SRe^{2}L	38.17	44.97	47.12	48.48	47.67	49.33	49.74	50.01	49.56	50.13
`CDA` (ours)	44.57	52.92	54.19	53.67	51.98	53.21	52.96	52.58	52.40	52.18

B.3 ImageNet-1K

Hyper-parameter Settings. We employ PyTorch off-the-shelf ResNet-18 and DenseNet-121 with the Top-1 accuracy of {69.8%, 74.4%} which are trained with the official recipe in Table 13a. And the recovery settings are provided in Table 13c, and it is noteworthy that we tune and set distinct parameters α_{BN} and learning rate for different recovery models in Table 13d. Then, we employ ResNet-{18, 50, 101, 152} (He et al., 2016), DenseNet-121 (Huang et al., 2017), RegNet (Radosavovic et al., 2020), ConvNeXt (Liu et al., 2022b), and DeiT-Tiny (Touvron et al., 2021) as validation models to evaluate the cross-model generalization on distilled ImageNet-1K dataset under the validation setting in Table 13b.

Table 13: Hyper-parameter settings on ImageNet-1K.

(a) Squeezing setting.

config	value
optimizer	SGD
base learning rate	0.1
momentum	0.9
weight decay	1e-4
batch size	256
lr step size	30
lr gamma	0.1
training epoch	90
augmentation	RandomResizedCrop

(b) Validation setting.

config	value
optimizer	AdamW
base learning rate	1e-3
weight decay	1e-2
batch size	128
learning rate schedule	cosine decay
training epoch	300
augmentation	RandomResizedCrop

(c) Shared recovery setting.

config	value
optimizer	Adam
momentum	β_1, β_2 = 0.5, 0.9
batch size	100
learning rate schedule	cosine decay
augmentation	RandomResizedCrop

(d) Model-specific recovery setting.

config	ResNet-18	DenseNet-121
α_{BN}	0.01	0.01
base learning rate	0.25	0.5
recovery iteration	1,000 / 4,000	1,000

Histogram Values. The histogram data of ImageNet-1K comparison with SRe2L in Figure 1 can be conveniently found in the following Table 14 for reference.

Table 14: ImageNet-1K comparison with SRe^{2}L. This table complements details in Figure 1.

Method \Validation Model	ResNet-18	ResNet-50	ResNet-101	DenseNet-121	RegNet-Y-8GF
SRe^{2}L (4K)	46.80	55.60	57.59	49.74	60.34
Our `CDA` (1K)	52.88	60.70	61.10	57.26	62.94
Our `CDA` (4K)	53.45	61.26	61.57	57.35	63.22

To conduct the ablation studies efficiently in Table 2, Table 19 and Figure 6, we recover the data for 1,000 iterations and validate the distilled dataset with a batch size of 1,024, keeping other settings the same as Table 13. Detailed values of the ablation study on schedulers are provided in Table 15.

Table 15: Ablation study on three different schedulers with varied milestone settings. It complements details in Figure 6.

Scheduler \ Milestone	0.1	0.2	0.3	0.4	0.5	0.6	0.7	0.8	0.9	1
Step	45.46	46.08	46.65	46.75	46.87	46.13	45.27	44.97	42.49	41.18
Linear	45.39	46.30	46.59	46.51	46.60	47.18	47.13	47.37	48.06	47.78
Cosine	45.41	45.42	46.15	46.90	46.93	47.42	46.86	47.33	47.80	48.05

Cross-Model Generalization. To supplement the validation models on distilled ImageNet-1K in Table 5, including more different architecture models to evaluate the cross-architecture performance. We have conducted validation experiments on a broad range of models, including SqueezeNet, MobileNet, EfficientNet, MNASNet, ShuffleNet, ResMLP, AlexNet, DeiT-Base, and VGG family models. These validation models are selected from a wide variety of architectures, encompassing a vast range of parameters, shown in Table 16. In the upper group of the table, the selected models are relatively small and efficient. There is a trend that its validation performance improves as the number of model parameters increases. In the lower group, we validated earlier models AlexNet and VGG. These models also show a trend of performance improvement with increasing size, but due to the simplicity of early model architectures, such as the absence of residual connections, their performance is inferior compared to more recent models. Additionally, we evaluated our distilled dataset on ResMLP, which is based on MLPs, and the DeiT-Base model, which is based on transformers. In summary, the distilled dataset created using our `CDA` method demonstrates strong validation performance across a wide range of models, considering both architectural diversity and parameter size.

Table 16: ImageNet-1K Top-1 on cross-model generation. Our `CDA` dataset consists of 50 IPC.

Model	SqueezeNet	MobileNet	EfficientNet	MNASNet	ShuffleNet	ResMLP
#Params (M)	1.2	3.5	5.3	6.3	7.4	30.0
accuracy (%)	19.70	49.76	55.10	55.66	54.69	54.18
Model	AlexNet	DeiT-Base	VGG-11	VGG-13	VGG-16	VGG-19
#Params (M)	61.1	86.6	132.9	133.0	138.4	143.7
accuracy (%)	14.60	30.27	36.99	38.60	42.28	43.30

B.4 ImageNet-21K

Hyper-parameter Setting. ImageNet-21K-P (Ridnik et al., 2021) proposes two training recipes to train ResNet-{18, 50} models. One way is to initialize the models from well-trained ImageNet-1K weight and train on ImageNet-21K-P for 80 epochs, another is to train models with random initialization for 140 epochs, as shown in Table 17a. The accuracy metrics on both training recipes are reported in Table 18. In our experiments, we utilize the pre-trained ResNet-{18, 50} models initialized by ImageNet-1K weight with the Top-1 accuracy of {38.1%, 44.2%} as recovery model. And the recovery setting is provided in Table 17c. Then, we evaluate the quality of the distilled ImageNet-21K dataset on ResNet-{18, 50, 101} validation models under the validation setting in Table 17b. To accelerate the ablation study on the batch size setting in Table 4, we train the validation model ResNet-18 for 140 epochs.

C Reverse Curriculum Learning

Reverse Curriculum Learning (RCL). We use a reverse step scheduler in the RCL experiments, starting with the default cropped range from β_l to β_u and transitioning at the milestone point to optimize the whole image, shifting from challenging to simpler optimizations. Other settings follow the recovery recipe on ResNet-18 for 1K recovery iterations. Table 19 shows the RCL results, a smaller step milestone indicates an earlier difficulty transition. The findings reveal that CRL does not improve the generated dataset's quality compared to the baseline SRe^{2}L, which has 44.90% accuracy.

Table 17: Hyper-parameter settings on ImageNet-21K.

(a) Squeezing setting.

config	value
optimizer	Adam
base learning rate	3e-4
weight decay	1e-4
batch size	1,024
learning rate schedule	cosine decay
label smooth	0.2
training epoch	80/140
augmentation	CutoutPIL, RandAugment

(b) Validation setting.

config	value
optimizer	AdamW
base learning rate	2e-3
weight decay	1e-2
batch size	32
learning rate schedule	cosine decay
label smooth	0.2
training epoch	300
augmentation	CutoutPIL, RandomResizedCrop

(c) Recovery setting.

config	value
α_{BN}	0.25
optimizer	Adam
base learning rate	0.05 (ResNet-18), 0.1 (ResNet-50)
momentum	β_1, $\beta_2 = 0.5, 0.9$
batch size	100
learning rate schedule	cosine decay
recovery iteration	2,000
augmentation	RandomResizedCrop

Table 18: Accuracy of ResNet-{18, 50} on ImageNet-21K-P.

Model	Initial Weight	Top-1 Acc. (%)	Top-5 Acc. (%)
ResNet-18 (Ours)	ImageNet-1K	38.1	67.2
	Random	38.5	67.8
Ridnik et al. (2021)	ImageNet-1K	42.2	72.0
ResNet-50 (Ours)	ImageNet-1K	$44.2^{\uparrow 2.0}$	$74.6^{\uparrow 2.6}$
	Random	$44.5^{\uparrow 2.3}$	$75.1^{\uparrow 3.1}$

Table 19: Ablation of reverse curriculum learning.

Step Milestone	Accuracy (%)
0.2	41.38
0.4	41.59
0.6	42.60
0.8	44.39

D Visulization

We provide additional comparisons of four groups of visualizations on synthetic ImageNet-21K images at recovery steps of {100, 500, 1,000, 1,500, 2,000} between SRe^{2}L (upper) and `CDA` (lower) in Figure 9. The chosen target classes are *Benthos*, *Squash Rackets*, *Marine Animal*, and *Scavenger*.

In addition, we present our `CDA`'s synthetic ImageNet-1K images in Figure 10 and ImageNet-21K images in Figure 11 and Figure 12.

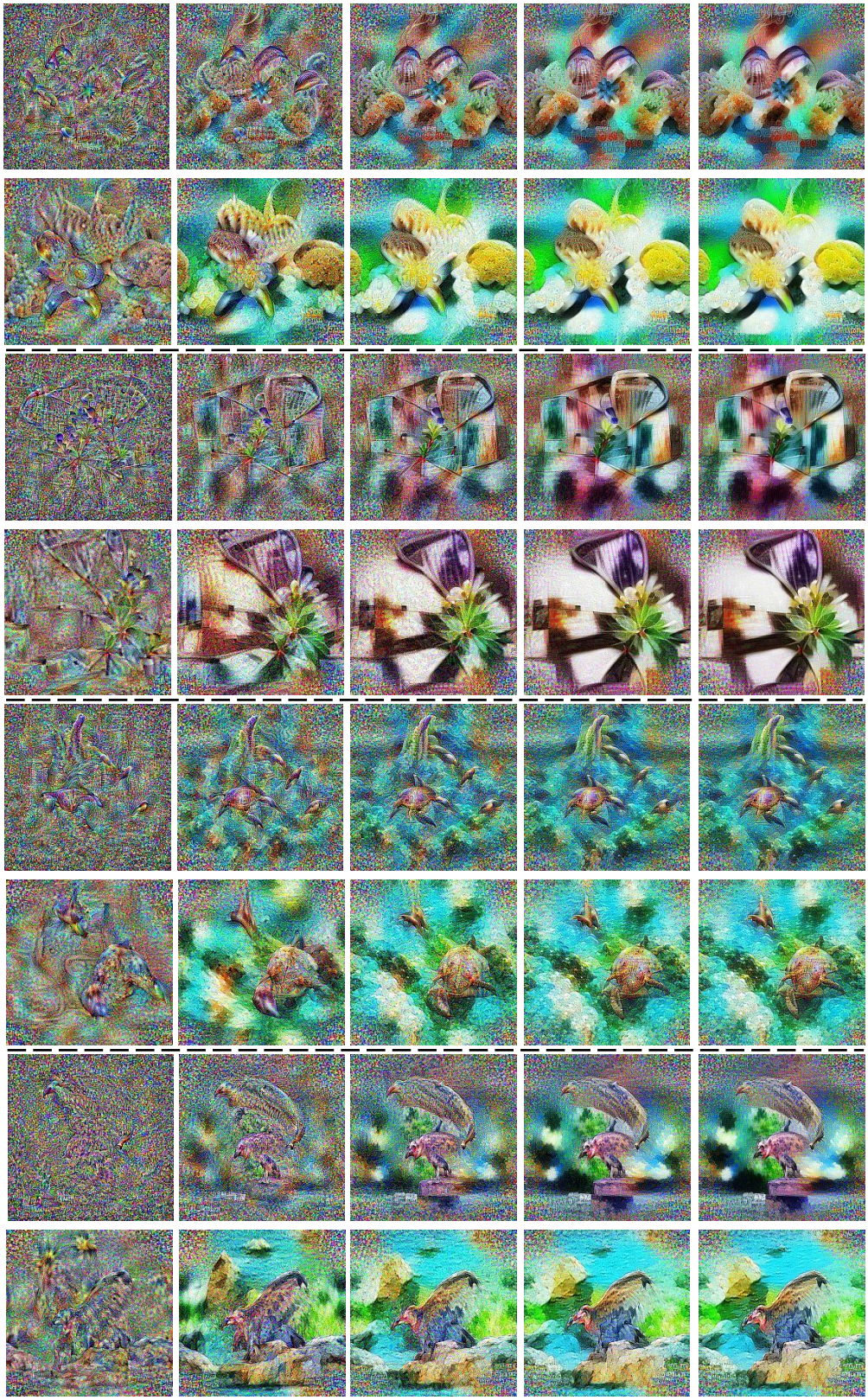

Figure 9: Synthetic ImageNet-21K data visualization comparison.

Figure 10: Synthetic ImageNet-1K data visualization from CDA.

Figure 11: Synthetic ImageNet-21K data distilled from ResNet-18 by `CDA`.

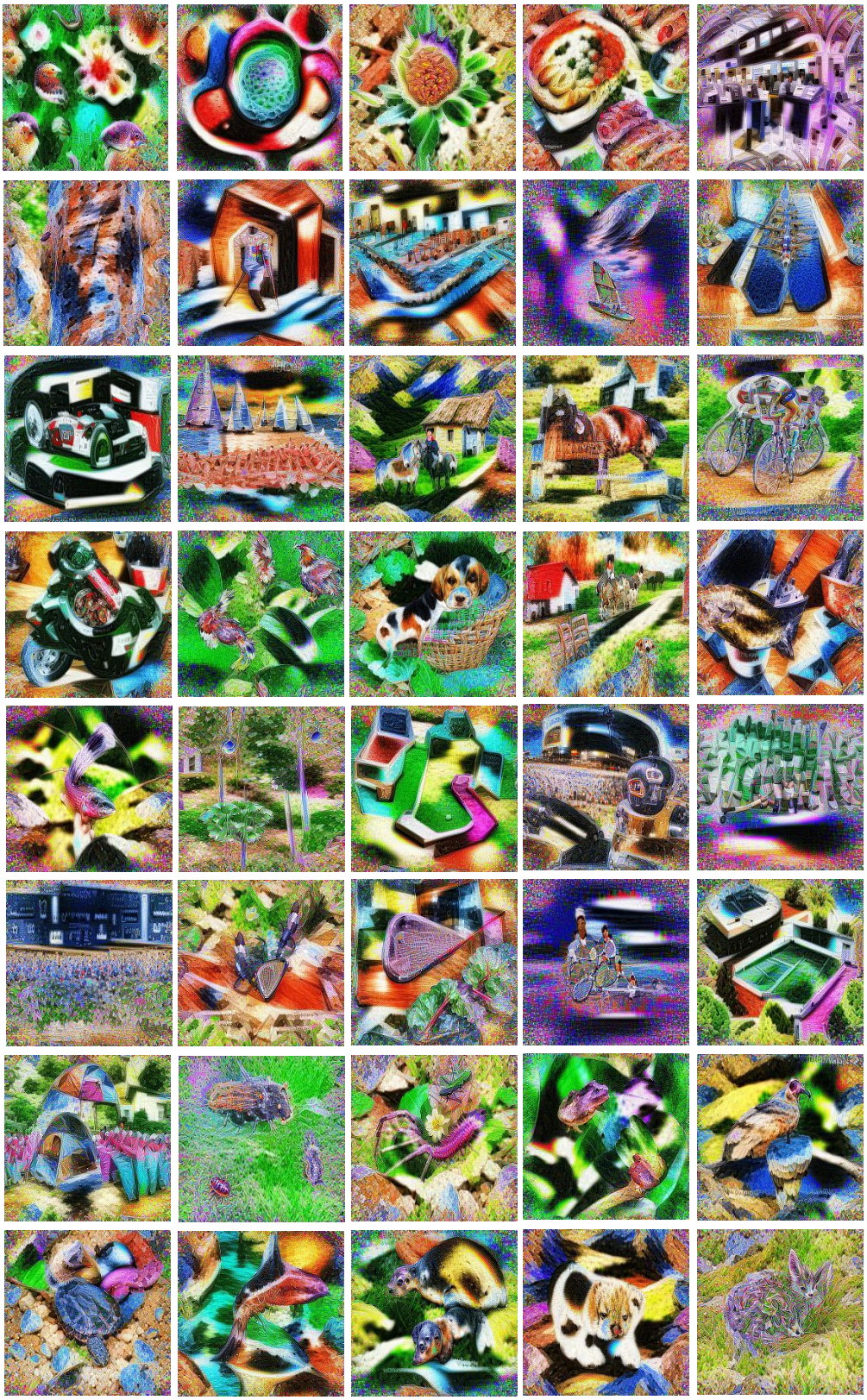

Figure 12: Synthetic ImageNet-21K data distilled from ResNet-50 by `CDA`.